Hysteresis and relaxation in bistable diffusive sandpile

I. Gruzinov, P. H. Diamond, and M. N. Rosenbluth
Department of Physics, University of California, San Diego, San Diego, California 92093

(Received 6 November 2002; accepted 22 November 2002)

Several problems in the physics of $L \rightarrow H$ transition and pedestal formation are examined using a simple and universal sandpile model, which incorporates key features of a confined plasma, namely, diffusion, shear induced bistability of turbulent transport, and a local magnetohydrodynamic (MHD) limit on the gradient. The main focus of this study is the effect of ambient diffusion, representative of neoclassical transport, on hysteresis and edge relaxation phenomena. The transport function of the sandpile bifurcates to a multivalued function with increasing deposition, and, as a consequence, a hysteresis in the $L \rightarrow H \rightarrow L$ transition is observed. With pedestal formation, diffusive losses increase at the expense of the turbulent flux. This effect prolongs the time needed to reach the MHD stability boundary, and thus provides a positive feedback on the pedestal. The gradient in the pedestal is more rigid and, due to diffusive smoothing, can reach the critical value at all radii simultaneously. Hence an avalanche, starting at the edge, can span the entire pedestal, thus destroying it. The transport in the core is essentially unaffected by the diffusion. © *2003 American Institute of Physics*. [DOI: 10.1063/1.1539032]

Recently[1] we presented a simple sandpile model as a vehicle for insight into the complex phenomenon of $L \rightarrow H$ transition and pedestal formation. This model suggests, that a second, "hard" local magnetohydrodynamic (MHD) instability is intrinsic to pedestal formation, while the suppression of the "background" turbulence is not. We further noted that the main effect of the pedestal on the transport processes is to truncate long-range avalanches and thus isolate the core region from the boundary. In the current paper we are mostly concerned with an effect of the diffusion on the dynamics of pedestal formation and relaxation. Diffusion appears to lead to a substantial hysteresis in the "transport function" of the sandpile model and to quasiperiodic large scale relaxation events, somewhat reminiscent of giant edge localized mode (ELM) discharges.[2,3] Both are similar to what is observed in experiments.[4,5]

Let us recall here how we designed the bistable sandpile: h_l is the height of the lth cell, $Z_l = h_l - h_{l+1}$ is a local slope. The slope is stable if $Z_l < Z_{c1}$ or $Z_{c2} < Z_l < Z_{c3}$. If $Z_{c1} \leqslant Z_l \leqslant Z_{c2}$, the slope is in the first unstable range, and D_z number of grains is transported downhill. If the slope exceeds the second, hard margin, i.e., $Z_{c3} \leqslant Z_l$, we topple $1 + (Z_l - Z_{c1})/2$ grains to relax Z_l to a subcritical value $Z_{c1} - 1$, see Fig. 1.

Now introduce a diffusive flux into the lth cell:[6] $\Gamma_l^D = D_0(Z_{l-1} - Z_l) = D_0(h_{l-1} - 2h_l + h_{l+1})$. With the natural boundary conditions $Z_L = h_L$ and $\Gamma_L = D_0(Z_{L-1} - Z_L)$ at the open boundary and $\Gamma_1 = -D_0 Z_1$ in the closed one, the *net* diffusive flux is $-D_0 Z_L$, corresponding to a net loss of sand because Z_L is positive. This intuitive means of introducing diffusion was benchmarked against a standard diffusion problem, and the sandpile model reproduces the analytical solution with a great accuracy. The sand pile is $L = 100$ cells wide and the constants Z_{c1}, Z_{c2}, Z_{c3}, and D_z are chosen to be 8, 20, 30, and 3. Variable parameters of the problem are a grain deposition rate N_f, varied from 1 to 10, and a diffusion coefficient D_0 varied from 0 to 0.16. The deposition profile in the sandpile model is uniform.

As for a nondiffusive sandpile, the diffusive sandpile undergoes transition from a state with a shallow profile (L-mode) to a state with a steep gradient (i.e., "pedestal") at the edge (H-mode) for sufficiently large deposition. Figure 2 shows steady-state profiles for a deposition rate $N_f = 5$ and for different values of diffusion coefficient D_0. The pedestal is clearly visible as a steepening of the sandpile near the edge for the diffusion coefficient less than ≈ 0.1.

The effect of the diffusion on the pedestal can be twofold. First, it smooths jumps in the gradient at the core–pedestal interface and at the open boundary. Second, it also prolongs the time needed to reach the hard instability boundary. For the case shown in Fig. 2, the second effect dominates for intermediate values of the diffusion coefficient, and as a result, for these values of D_0 the diffusive sandpile is *taller* than a nondiffusive pile, contrary to naive intuition. We observe that, as in the nondiffusive case, the slope in the pedestal is insensitive to the deposition. The slope slightly grows linearly with diffusion from $Z \approx 23$ for $D_0 = 0$ to $Z \approx 27$ for $D_0 = 0.1$.

Figure 3 shows the steady-state width of the pedestal as a function of the deposition rate for a diffusion coefficient fixed to $D_0 = 0.08$. One can see that, for $N_f = 5$, which is the case in Fig. 2, the width is approximately 40 cells when $D_0 = 0$, and approximately 60 cells when $D_0 = 0.08$. Thus, ambient diffusion is clearly seen to impact both the width and height of the pedestal; the pile becomes taller precisely because the pedestal becomes *wider* and *steeper*.

In contrast to the nondiffusive case, which has only one transport channel, corresponding to turbulent transport, in the diffusive model the sand is transported by turbulence *and* by diffusion. As a consequence of this two-channel transport, for some D_0 there exists a range of deposition rates N_f (called the "transition range") over which the sand pile re-

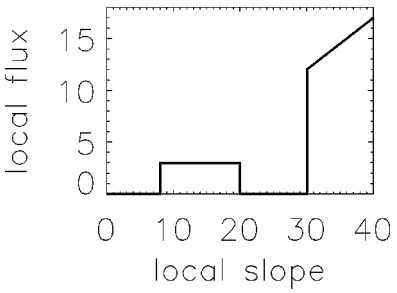

FIG. 1. Local flux Γ_l^T transported downhill when the local slope Z_l is unstable.

laxes to a state with or without pedestal, depending on initial conditions. For example, if we fix the diffusion to $D_0=0.08$, and vary N_f from 1 to 8 and back to 1, we observe that the pedestal appears at $N_f\approx 4$ and disappears at $N_f\approx 2$, as seen in Fig. 3.

Let us consider a "transport function" of our model, that is, the local flux $\Gamma(R)$ as a function of the local slope $Z(R)$, where R is the radius. The transport function can be presented graphically as a parametric plot of the *net* local flux $\Gamma_l=N_f l/L$ versus the *net* local slope Z_l, as done in Figs. 4 and 5. Transport functions of the nondiffusive and weakly diffusive sandpile models are qualitatively the same, as seen from Fig. 4. With increasing diffusion, a *bifurcation* of the transport function is observed. A hysteresis loop appears in $\Gamma(Z)$ as shown in Fig. 5 for the case of $D_0=0.08$. Obviously, the "transitional range" for the deposition rate is a direct reflection of this hysteresis.

Hysteresis is a characteristic feature of the diffusive sand pile for intermediate values of the diffusion coefficient, when the diffusive flux dominates in the H-mode, while the turbulent flux dominates in the L-mode. This allows some range of flux which can be transported by different combinations of Γ^D and Γ^T, depending on the confinement mode. E.g., for the case of $D_0=0.08$ (Fig. 5), the deposited flux $N_f=3$ can be transported either by $\Gamma^D=2.1$ (H-mode, the pedestal, $Z_L=26$) plus what is leftover by $\Gamma^T=0.9$, or by $\Gamma^D=0.7$ (L-mode, no pedestal, $Z_L=9$) plus $\Gamma^T=2.3$. *Hysteresis is not possible when one of the two transport channels dominates in both modes*, i.e., when the diffusion is too weak and Γ^T dominates (as in Ref. 1), or too strong and Γ^D dominates.

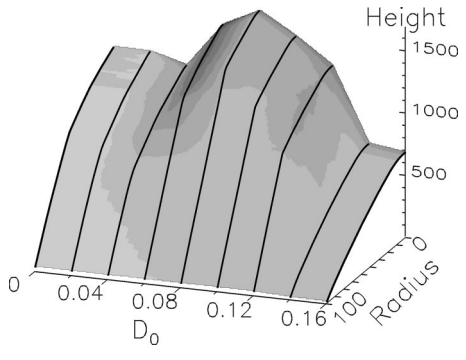

FIG. 2. Steady-state profiles of the sand pile for diffusion coefficient $D_0=0,0.02,\ldots,0.16$ and deposition rate $N_f=5$. Three regimes are obvious: (i) small diffusion, $D_0\leqslant 0.04$, causes profile smoothing; (ii) intermediate diffusion, $0.06\leqslant D_0\leqslant 0.12$, the diffusive pile is higher than the nondiffusive one; (iii) large diffusion $D_0\geqslant 0.14$ prevents the edge steepening, or, more precisely, the deposition $N_f=5$ is not sufficient for pedestal formation when $D_0\geqslant 0.14$. The top of the pile is flattened by diffusion.

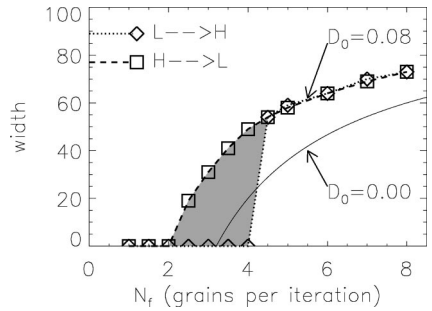

FIG. 3. Width of the pedestal in the simulations for different deposition rates and with the diffusion coefficient fixed to $D_0=0.08$. Shaded is a "transition region" over which the pedestal does not appear if the simulations were initialized with a shallow profile, but does appear if the simulations were initialized with a steep one. The threshold for $L\rightarrow H$ transition is $N_f=4$, and for reverse transition $H\rightarrow L$ the threshold is $N_f=2$. The solid line (for reference) represents $w(N_f)$ for a nondiffusive case.

Figure 6 illustrates the whole $L\rightarrow H\rightarrow L$ cycle: start with a small deposition $N_f=2$ below the transition threshold, then gradually increase deposition until $N_f=5$ well above the transition range, then gradually turn off the deposition, *always* allowing the pile to relax into the stationary state. The diffusion is fixed at the value of $D_0=0.08$. Steady-state patterns of avalanches are shown for four cases: L-modes below, and in, the $L\rightarrow H$ hysteresis loop, and H-mode above, and in, the $H\rightarrow L$ loop. In the L-mode (absence of the pedestal), the transport through the edge is driven by the "first instability," complemented by weak diffusive losses. In the H-mode (with the pedestal), the diffusive losses are substantial (equal to $D_0 Z_L$), and exceed the transport by rare edge bursts of "hard" instability in the pedestal, as seen in Fig. 6(c). Note, both panels on the right depict the $N_f=3$ case to illustrate the hysteresis in the $L\rightarrow H\rightarrow L$ cycle: case (b) is L-mode on the $L\rightarrow H$ branch, and case (d) is H-mode on the $H\rightarrow L$ branch. From Figs. 5 and 6, the effect of the diffusion on transport processes can be summarized as follows: Starting from a shallow profile and increasing the grain deposition rate, we expect the sandpile to start steepening near the open edge when the deposition exceeds the maximal flux that

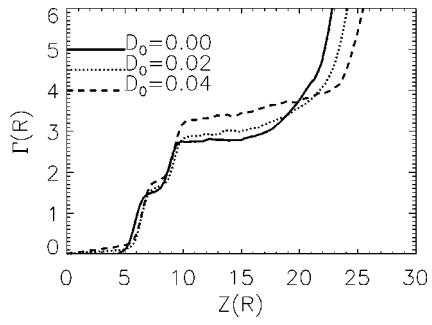

FIG. 4. Transport functions of the nondiffusive and weakly diffusive sandpile models are very similar. The threshold deposition for $L\rightarrow H$ transition and reverse (no hysteresis) is the value of flux Γ, at which the transport function inflects: $\Delta\Gamma/\Delta Z=0$. This value slightly grows with diffusion.

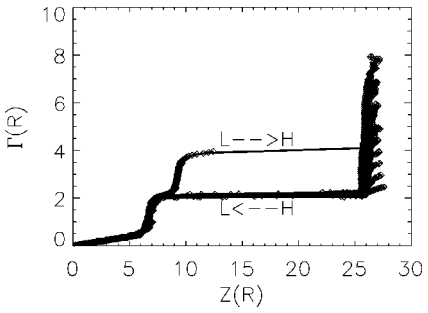

FIG. 5. Transport function for the case of $D_0=0.08$ shows a hysteresis in $L\rightarrow H\rightarrow L$ transitions. Observe, that the "inflection region" $\Delta\Gamma/\Delta Z=0$ is larger in ΔZ, and the slope in the pedestal is more "rigid" (i.e., $\Delta\Gamma/\Delta Z\rightarrow\infty$) than these in the nondiffusive case.

can be transported by the background turbulence *plus* diffusion. Thus, the threshold for the $L\rightarrow H$ transition is always higher than that in the nondiffusive case. Once the pedestal is formed, the diffusive flux becomes substantial and, if the deposition rate is not far above the threshold value, little flux is left to be transported by the "hard" instability. Moreover, the diffusive smoothing of the slope inhomogeneity prevents edge steepening, and instead causes homogeneous growth of the pedestal. As a result, long periods of edge quiescence (except for a constant diffusive flux), interspersed by infrequent avalanches of the distinctive "triangular" space–time pattern are observed. Once the H-mode is established, the deposition rate can be reduced without destroying the pedestal as long as the deposition exceeds the diffusive flux. If the deposition becomes smaller than that, the pedestal disappears.

The crucial role of the second stable range of slopes (corresponding to suppression of the turbulent transport) is apparent: it allows the diffusion to take over the transport while keeping the pedestal in the stable range of slopes for a long time. Indeed, we do not observe the hysteresis in the runs with $Z_{c2}=29$, i.e., without second stability. In this case, the threshold deposition rate for $L\rightarrow H$ and reverse transitions simply grows with the diffusion (actually, the threshold for $L\rightarrow H$ transition is a function of diffusion coefficient D_0 and size of a flip D_z, and is independent of other parameters of the model). Again, as in the nondiffusive case, second stability (and transport bifurcation) is not essential for the pedestal formation, though the pedestal is smoothed by the diffusion and the diffusive pile is lower than the nondiffusive one.

There are many ways to define some function that would characterize the transport activity in the pile. The main purpose of such a function is to illustrate spectrum, which is a characteristic of the critical state. Indeed, the definition of the critical state itself is that there exists a function of this state which shows a power-law spectrum. We adopt the total number of unstable cells at each time, $g(t)$, as a function whose statistical properties, namely, probability density function (PDF) and a spectrum, we wish to study. This function characterizes the turbulence activity, leaving aside the diffusive dissipation.

Let us take another look at Figs. 6(a) and 6(b), which show two cases of L-mode as explained above. The power spectra of $g(t)$ exhibit a flat low-frequency region followed by an ω^{-1} region and high-frequency tail ω^{-3}. The auxiliary lines, which show the power-law fits, are drawn identically in both power spectrum plots of Fig. 6. This allows us to observe that the power content of turbulence shifts toward higher frequencies with increasing deposition. The existence of ω^{-1} suggests a range of correlated scales. Varying the size of the sandpile L, we found that the low and high frequency limits of the ω^{-1} region are locked to the system size as $1/L$ and $3/L$, as shown in Figs. 6(a) and 6(b). Since an elementary transport event proceeds at the cell scale in one iteration, the ω^{-1} spectrum truly represents a long-range phenomena. This is not the case for the ω^{-3} spectrum, since its high-frequency limit coincides with the Nyquist frequency $(2\,iteration)^{-1}$, a microscale of the problem. It is also worth noting the absence of any intermediate, transitional scaling between the -1 and -3 power laws.

Similar to the nondiffusive H-mode, the power spectra in two H-modes shown in Figs. 6(c) and 6(d) do not have an ω^{-1} scaling. Rather, a flat low-frequency region is followed by the $\omega^{-2.5}$ tail. In contrast to the nondiffusive case, in which the power index in the H-mode is almost twice as small as that in the L-mode (being system-size independent in both modes), for the case of finite diffusion the index depends on the system size (ranging from -2.5 for $L=100$ cells to -3 for $L=300$ cells for $D_0=0.08$). This is attributed mainly to the fact that the diffusion, being a second order spatial derivative, induces a correlation at scales larger than the turbulence scales, but smaller than the system size. This is consistent with the observation that the power index increases with system size in the H-mode, where diffusive losses are substantial, but is independent of the system size in the L-mode, where diffusive losses are not important. Thus one can appreciate the existence of the system-size independent power-law spectrum as a nontrivial case.

It is instructive to compare cases of $N_f=3$ without and with the pedestal, as in Figs. 6(b) and 6(c). First, the pedestal [case (c)] contributes little to the function $g(t)$, since most of the time it is stable, but the ω^{-1} power law is gone. This is so because the ω^{-1} law of $g(t)$ in the L-mode is due to the *overlapping* of the individual avalanches. This takes place at large radii, near the edge, where the flux is large. The presence of the pedestal eliminates that region, but does not affect the core. Thus, the pattern of avalanches in the core regions is the same in both modes. Second, that the cutoff frequency for the power law is exactly $1/L$ means that avalanches of all sizes (up to the size of the sandpile), are present, and that the power content in scales larger than the size of the pile is scale-independent. On the other hand, in the case of a large, statistically significant pedestal, as in Fig. 6(d), the power law persists at frequencies below $1/L$ (although L is the only macroscopic scale length present in the system). This is because a long time is required for the pedestal to reach the critical gradient, as explained above. In this case, the characteristic time for $g(t)$ is determined by the diffusion and deposition rate, but not by the time needed for an avalanche to span the entire sandpile! Also, because space–time patterns of avalanches in the pedestal has a tri-

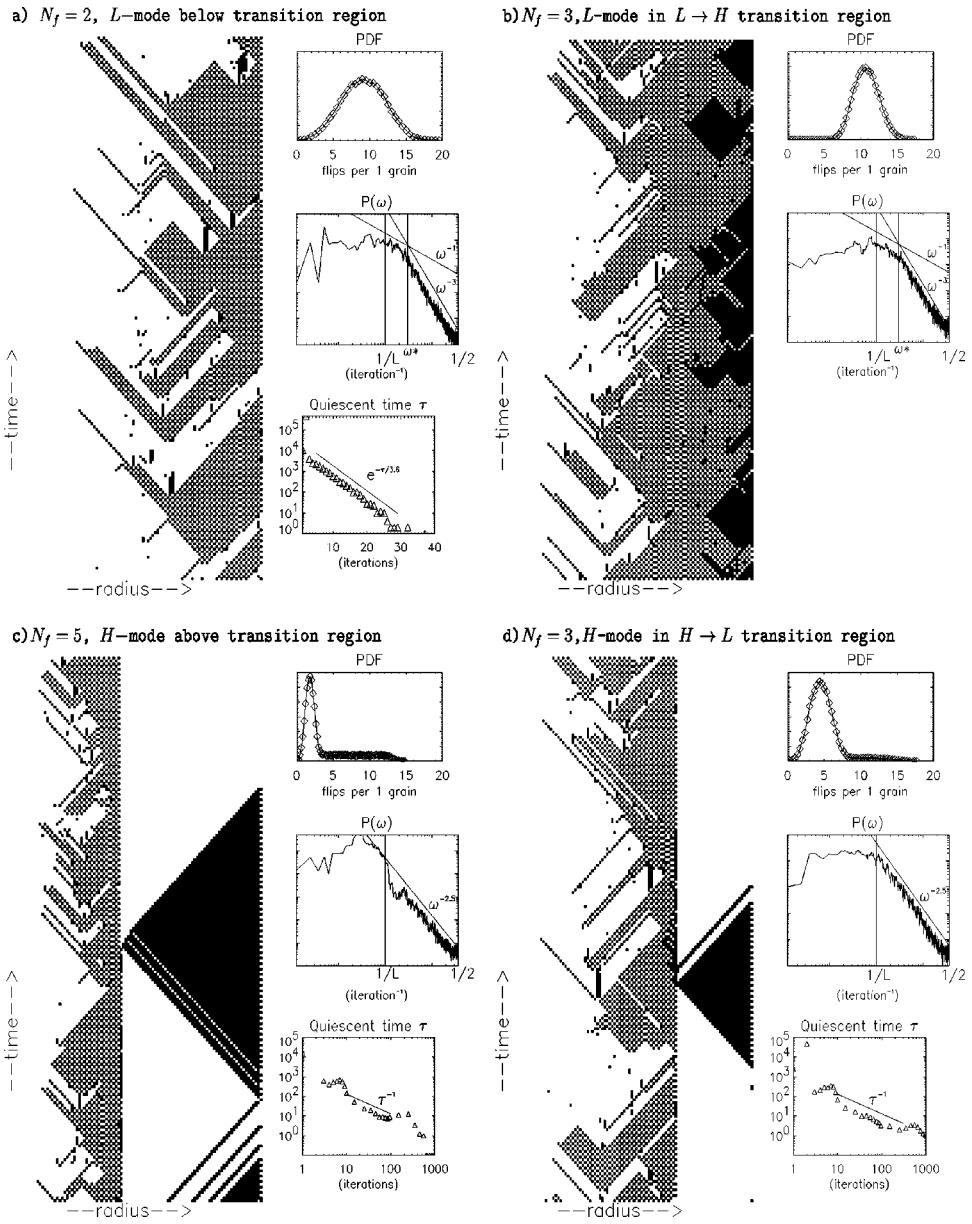

FIG. 6. The space–time pattern of the pile: white cells are stable, gray and black cells are in first and in second unstable ranges of slopes, respectively. On the right at each of the panels, the power spectrum and PDF of total number of flips are shown. Also plotted is the distribution of quiescent time between edge events.

angular shape, all scales (from 1 cell to the pedestal width) are present with the same probability. That uniform probability shows up in PDF as a long and *flat* appendix to the Gaussian.

Finally, Figs. 6(a), 6(c), 6(d) show the edge quiescent time distribution. In L-mode it is exponential, in H-mode it is approximately power law between two Gaussians. Second maxima are at 500 and at 200 time steps for cases $N_f = 3$ and $N_f = 5$, respectively.

In conclusion, a simple bistable sandpile model with diffusion was utilized to elucidate certain key features of $L \to H \to L$ transitions. The main conclusion we draw from this study is that *both* diffusion and second stability are necessary for the appearance of hysteresis in the transport function of the model and in the $L \to H \to L$ thresholds. Furthermore, hysteresis is observed only when turbulent and diffusive fluxes are *comparable*. This differs from the common intuition based on simple models.[7,8] The effect of the diffusion on the pedestal structure and dynamic is substantial. First, the pedestal can be wider and taller with diffusion than without. Second, large edge discharges are rare and span the whole pedestal, thus resembling giant ELMs. Such large discharge events were not observed in sandpile models without diffusion.

The authors thank A. Hubbard, M. Malkov, D. Newman, and M. Shats for useful discussions.

The research was supported by DOE Grant No. DE-FG03-88ER53275.

[1] I. Gruzinov, P. H. Diamond, and M. N. Rosenbluth, Phys. Rev. Lett. **89**, 255001 (2002).
[2] H. Zohm, Plasma Phys. Controlled Fusion **38**, 105 (1996).
[3] J. W. Connor, Plasma Phys. Controlled Fusion **40**, 531 (1997).
[4] A. E. Hubbard, Plasma Phys. Controlled Fusion **42**, A15 (2000).
[5] D. M. Thomas, R. J. Groebner, K. H. Burrell, T. H. Osborne, and T. N. Carlstrom, Plasma Phys. Controlled Fusion **40**, 707 (1997).
[6] R. Sanchez, D. E. Newman, and B. A. Carreras, Nucl. Fusion **41**, 247 (2001).
[7] H. Biglari, P. Diamond, and P. W. Terry, Phys. Fluids B **2**, 1 (1990).
[8] F. I. Hinton, Phys. Fluids B **3**, 696 (1991).